



**Strain effects on the topological and valley properties of the Janus monolayer VSiGeN<sub>4</sub>**San-Dong Guo <sup>1</sup>, Wen-Qi Mu,<sup>1</sup> Jia-Hao Wang,<sup>1</sup> Yu-Xuan Yang,<sup>1</sup> Bing Wang <sup>2</sup> and Yee-Sin Ang<sup>3</sup><sup>1</sup>*School of Electronic Engineering, Xi'an University of Posts and Telecommunications, Xi'an 710121, China*<sup>2</sup>*Institute for Computational Materials Science, School of Physics and Electronics, Henan University, Kaifeng 475004, China*<sup>3</sup>*Science, Mathematics and Technology, Singapore University of Technology and Design, 8 Somapah Road, Singapore 487372, Singapore*

(Received 21 May 2022; revised 19 July 2022; accepted 2 August 2022; published 11 August 2022)

Strain is an effective method to tune the electronic properties of two-dimensional (2D) materials and can induce novel phase transition. Recently, the 2D  $MA_2Z_4$  family of materials has attracted interest because of their emerging topological, magnetic, and superconducting properties. Here, we investigate the impact of strain effects ( $a/a_0 = 0.96\text{--}1.04$ ) on the physical properties of the Janus monolayer VSiGeN<sub>4</sub> as a derivative of VSi<sub>2</sub>N<sub>4</sub> or VGe<sub>2</sub>N<sub>4</sub>, which possesses dynamical, mechanical, and thermal stabilities. For out-of-plane magnetic anisotropy, with increasing strain, VSiGeN<sub>4</sub> undergoes a transition between a ferrovalley semiconductor (FVS), half-valley metal (HVM), valley-polarized quantum anomalous Hall insulator, HVM, and FVS. These effects imply twice topological phase transitions, which are related to the sign-reversible Berry curvature and band inversion between  $d_{xy} + d_{x^2-y^2}$  and  $d_{z^2}$  orbitals for the  $K$  or  $-K$  valley. The band inversion also leads to transformation of valley splitting strength between the valence and conduction bands. However, for in-plane magnetic anisotropy, no special quantum anomalous Hall (QAH) states and valley polarization exist within the considered strain range. The actual magnetic anisotropy energy shows no special QAH and HVM states in monolayer VSiGeN<sub>4</sub>. Fortunately, these can easily be achieved by an external magnetic field, which adjusts the easy magnetization axis of VSiGeN<sub>4</sub> from an in-plane one to an out-of-plane one. Our findings shed light on how strain can be employed to engineer the electronic states of VSiGeN<sub>4</sub>, which may lead to new perspectives on multifunctional quantum devices in valleytronics and spintronics.

DOI: [10.1103/PhysRevB.106.064416](https://doi.org/10.1103/PhysRevB.106.064416)**I. INTRODUCTION**

Magnetism of two-dimensional (2D) systems is one of the most fascinating properties of materials due to its interplay with other important properties of materials such as superconductivity, ferrovalley (FV), ferroelectricity, piezoelectricity, and quantum anomalous Hall (QAH) effects. However, based on the Mermin-Wagner theorem, long-range magnetic order is prohibited in a 2D system [1]. Fortunately, the 2D intrinsic long-range ferromagnetic (FM) order semiconductors Cr<sub>2</sub>Ge<sub>2</sub>Te<sub>6</sub> and CrI<sub>3</sub> have been achieved experimentally, obtained from their van der Waals layered bulk materials [2,3], due to the stabilization of FM order by magnetic anisotropy. In addition, the direction of magnetic anisotropy has an important effect on the topological and valley properties of some 2D materials because it can affect the symmetry of such 2D systems [4–7]. For example, in monolayer RuBr<sub>2</sub>, FV to half-valley metal (HVM) to QAH to HVM to FV transitions can be induced by increasing the electron correlation  $U$  with a fixed out-of-plane magnetic anisotropy, but no special QAH states and valley polarization can be observed for the in-plane case [7]. Thus, it may be very interesting to tune the magnetic anisotropy of 2D systems by an external field, such as biaxial strain, an electric field, and correlation effects.

Strain engineering is an important strategy for tuning the electronic, topological, thermoelectric, piezoelectric, and magnetic properties of 2D materials and has been widely used

in the modulation of physical and chemical properties [8]. The QAH state in VN<sub>2</sub>X<sub>2</sub>Y<sub>2</sub> nanosheets ( $X = \text{B-Ga}$ ,  $Y = \text{O-Te}$ ) can be induced by strain, and the valley polarization can also be switched from the bottom conduction band to the top valence band [9]. For monolayer  $M\text{Br}_2$  ( $M = \text{Ru and Os}$ ), compressive strain can induce phase transitions in materials from a ferrovalley semiconductor (FVS) to HVM to a valley-polarized quantum anomalous Hall insulator (VQAH) to HVM to FVS [10]. However, in these works, the intrinsic MAE as a function of strain has not been considered, and out-of-plane magnetic anisotropy is assumed to be fixed within the considered strain range. Our recent works show that an increasing strain can induce switching of the magnetic anisotropy from an out-of-plane one to an in-plane one [7], thus producing manifold electronic states. Thus, strain engineering may produce a complex phase transition of electronic states by tuning the magnetic anisotropy.

In 2020, septuple-atomic-layer 2D MoSi<sub>2</sub>N<sub>4</sub> and WSi<sub>2</sub>N<sub>4</sub> were successfully synthesized by the chemical vapor deposition method [11]. Subsequently, the 2D  $MA_2Z_4$  family with a septuple-atomic-layer structure was constructed by intercalating a MoS<sub>2</sub>-type monolayer  $MZ_2$  into an InSe-type monolayer  $A_2Z_2$ , and the family possesses emerging topological, magnetic, valley, superconducting, and electrical contact properties [12–14]. Then, Janus 2D materials in the new 2D  $MA_2Z_4$  family were proposed, such as MSiGeN<sub>4</sub> ( $M = \text{Mo and W}$ ) and SrAlGaSe<sub>4</sub>, and some novel properties can

be achieved in these Janus materials, such as Rashba spin splitting and out-of-plane piezoelectric polarization [15,16]. Recently, the Janus VSiGeN<sub>4</sub> monolayer was predicted to be a thermodynamically stable intrinsic 2D ferromagnet [17].

In this work, we investigate the strain effects on the topological and valley properties of the Janus VSiGeN<sub>4</sub> monolayer and reveal the importance of magnetic anisotropy in determining its magnetic, topological, and valley properties. It is found that different strain strengths can drive the system into different novel electronic states (FVS, HVM, and VQAH) in a fixed out-of-plane case, enabling a rich phase diagram. However, for the in-plane case, only common magnetic states appear. Due to weak spin-orbit coupling (SOC) in VSiGeN<sub>4</sub>, the magnetic shape anisotropy (MSA) induced by the magnetic dipolar interaction can overcome the magnetocrystalline anisotropy (MCA) to evince an easy plane in the considered strain range. So strained VSiGeN<sub>4</sub> is intrinsically a common magnetic semiconductor. However, these topological and valley states can be achieved by a small external magnetic field. With increasing  $a/a_0$ , the MCA energy first switches from in plane to out of plane. Further increasing  $a/a_0$  will drive two additional transitions in the MCA from out of plane to in-plane to out of plane. Several transitions in the MCA are further identified by calculating MCA versus  $U$ . Our work highlights the role of magnetic anisotropy for VSiGeN<sub>4</sub> and deepens our understanding of strain along with magnetic anisotropy induced topological and valley states.

The rest of this paper is organized as follows. In the next section, we give our computational details and methods. In the following sections, we present the structure and stabilities, electronic states, and strain effects on physical properties of the VSiGeN<sub>4</sub> monolayer. Finally, we give our discussion and conclusion.

## II. COMPUTATIONAL DETAILS

Within density-functional theory (DFT) [18], we perform spin-polarized first-principles calculations by employing the projector augmented wave method, as implemented in the VASP code [19–21]. The generalized gradient approximation (GGA) of Perdew, Burke, and Ernzerhof [22] is adopted as the exchange-correlation functional. An energy cutoff of 500 eV, total energy convergence criterion of  $10^{-8}$  eV, and force convergence criteria of less than  $0.0001$  eV  $\text{\AA}^{-1}$  on each atom are used to attain accurate results. A vacuum space of more than 30  $\text{\AA}$  is used to avoid interactions between the neighboring slabs.  $\Gamma$ -centered  $16 \times 16 \times 1$   $k$ -point meshes are sampled in the Brillouin zone (BZ) for structure optimization, electronic structures, and the elastic stiffness tensor, and  $9 \times 16 \times 1$  Monkhorst-Pack  $k$ -point meshes are sampled for FM/antiferromagnetic (AFM) energy with a rectangle supercell. The on-site Coulomb correlation of V atoms is considered using the GGA+ $U$  method within the rotationally invariant approach proposed by Dudarev *et al.* [23], and  $U = 3.2$  eV is used, which was also used in Ref. [17]. The SOC effect is explicitly included to investigate MCA and the electronic and topological properties of the VSiGeN<sub>4</sub> monolayer.

The vibrational properties are investigated using the finite-displacement method with a  $5 \times 5 \times 1$  supercell, as

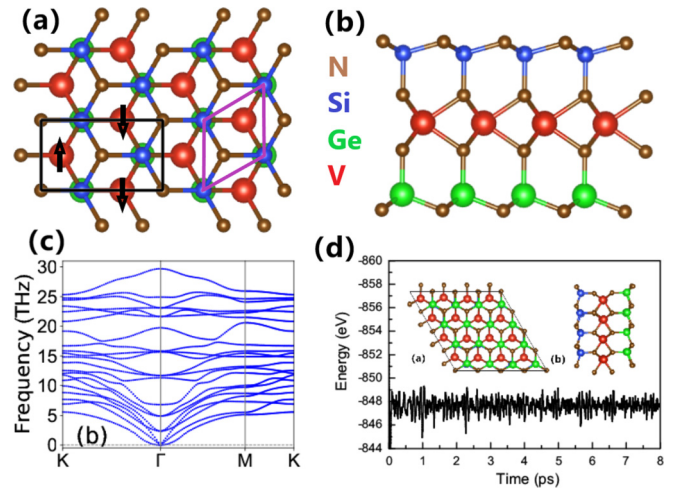


FIG. 1. VSiGeN<sub>4</sub> monolayer. (a) Top view and (b) side view of the crystal structure. The primitive cell (rectangle supercell) is shown by purple (black) lines, and the AFM configuration is marked with black arrows in (a). (c) The phonon dispersion curves. (d) The total energy fluctuations as a function of simulation time at 300 K; insets show the final structures [top view in (a) and side view in (b)] of VSiGeN<sub>4</sub> after 8 ps at 300 K.

implemented in the PHONOPY code [24]. We use the strain-stress relationship to attain the elastic stiffness tensor  $C_{ij}$ , and the 2D elastic coefficients  $C_{ij}^{2D}$  have been renormalized by  $C_{ij}^{2D} = L_z C_{ij}^{3D}$ , where  $L_z$  is the cell height along the  $z$  direction. The Berry curvatures are calculated directly from wave functions based on Fukui’s method [25], as implemented in the VASPBERRY code [26,27]. The mostly localized Wannier functions, including the  $d$  orbitals of the V atom and the  $p$  orbitals of Si, Ge, and N atoms, are constructed on a  $16 \times 16 \times 1$   $k$  mesh and then are used to calculate edge states using the WANNIER90 and WANNIERTOOLS packages [28,29]. The energy band structures of VSiGeN<sub>4</sub> calculated using DFT and fitted by WANNIER90 at  $a/a_0 = 0.993$  (in the topological state) are plotted in Fig. 1 [30], which confirms the fitting accuracy.

## III. STRUCTURE AND STABILITIES

As shown in Fig. 1, the structure of the VSiGeN<sub>4</sub> monolayer is stacked with seven atomic layers, N-Si-N-V-N-Ge-N. This can be regarded as a sandwich structure, and the middle VN<sub>2</sub> layer is sandwiched by SiN and GeN bilayers, which can be considered a Janus structure. The VSiGeN<sub>4</sub> monolayer can be built by replacing the Si/Ge atoms of one of the two SiN/GeN bilayers in the VSi<sub>2</sub>N<sub>4</sub>/VGe<sub>2</sub>N<sub>4</sub> monolayer with Ge/N atoms. The symmetry of VSiGeN<sub>4</sub> (No. 156) is lower than that of VSi<sub>2</sub>N<sub>4</sub>/VGe<sub>2</sub>N<sub>4</sub> (No. 187) due to the lack of the reflection symmetry with respect to the middle VN<sub>2</sub> layer. The rhombus primitive cell and the rectangle supercell are plotted in Fig. 1(a) along with the AFM configuration, and the first BZ with high-symmetry points is shown in Fig. 2 [30]. The optimized lattice constant  $a$  of the VSiGeN<sub>4</sub> monolayer is 2.959  $\text{\AA}$  with FM ordering, which agrees well with the previous theoretical value (2.97 $\text{\AA}$ ) [17].

Our calculations show that VSiGeN<sub>4</sub> stabilizes into a FM ground state, and the FM state is 125.7 meV lower in energy

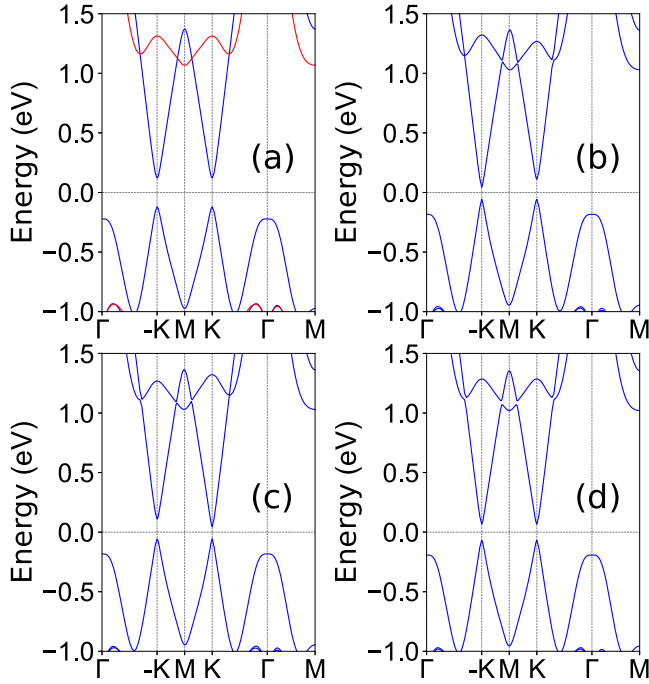


FIG. 2. Energy band structures of VSiGeN<sub>4</sub> (a) without SOC and (b)–(d) with SOC for the magnetic moment of V along the positive  $z$ , negative  $z$ , and positive  $x$  directions, respectively. In (a), the blue (red) lines represent the band structure in the spin-up (spin-down) direction.

than its AFM state with the rectangle supercell. The MAE includes two main terms [31–34]: (1) MCA energy  $E_{MCA}$ , which is induced by the SOC, and (2) MSA energy  $E_{MSA}$ , which is due to the dipole-dipole (D-D) interaction:

$$E_{D-D} = -\frac{1}{2} \frac{\mu_0}{4\pi} \sum_{i \neq j} \frac{1}{r_{ij}^3} \left[ \vec{M}_i \cdot \vec{M}_j - \frac{3}{r_{ij}^2} (\vec{M}_i \cdot \vec{r}_{ij})(\vec{M}_j \cdot \vec{r}_{ij}) \right], \quad (1)$$

where  $\vec{M}_i$  represents the local magnetic moments and  $\vec{r}_{ij}$  are vectors that connect sites  $i$  and  $j$ .  $E_{MCA}$  is calculated from an energy difference between in-plane magnetization and out-of-plane magnetic anisotropy within SOC. The calculated  $E_{MCA}$  of VSiGeN<sub>4</sub> is only  $-3 \mu\text{eV}$ . For most materials, the magnetic D-D interaction is small compared with the MCA interaction. However, for VSiGeN<sub>4</sub>, it may play an important role due to very small  $E_{MCA}$ . According to Fig. 1,  $E_{MSA}$  is calculated from an energy difference with the magnetization rotating from the in-plane direction to the out-of-plane direction. The calculated  $E_{MSA}$  is  $-17 \mu\text{eV}$ , which agrees well with the recently reported value of  $-16 \mu\text{eV}$  [17]. It is found that  $E_{MSA}$  dominates the MAE ( $-20 \mu\text{eV}$ ). Positive (negative) MAE means that the easy magnetization axis is perpendicular (parallel) to the plane of the monolayer. The calculated MAE indicates in-plane easy magnetization, which means that there is no energetic barrier to the rotation of magnetization in the  $xy$  plane [35]. So VSiGeN<sub>4</sub> can be considered a 2D  $XY$  magnet [35,36]. For a 2D  $XY$  magnet with a typical triangle lattice structure, a Berezinskii-Kosterlitz-Thouless magnetic transition to a quaslong-range phase will be produced at a

critical temperature. The Monte Carlo simulations have predicted the critical temperature  $T_C = 1.335 \frac{J}{K_B}$  [37,38], where  $J$  is the nearest-neighbor exchange parameter and  $K_B$  is the Boltzmann constant.  $J$  is determined from the energy difference between AFM energy  $E_{AFM}$  and FM energy  $E_{FM}$ . Based on the FM and AFM configurations, the AFM and FM energies can be obtained with the following equations:

$$E_{FM} = E_0 - (6J + 2A)S^2, \quad (2)$$

$$E_{AFM} = E_0 + (2J - 2A)S^2, \quad (3)$$

where  $E_0$  is the total energy of the systems without magnetic coupling and  $A$  describes the easy-axis single-ion anisotropy. The corresponding  $J$  can be obtained as

$$J = \frac{E_{AFM} - E_{FM}}{8S^2}. \quad (4)$$

The calculated  $J$  is 31.43 meV ( $S = \frac{1}{2}$ ), and  $T_C$  is estimated to be 487 K.

The dynamical stability of VSiGeN<sub>4</sub> is verified by its phonon band dispersion, which is presented in Fig. 1(c). Phonon branches show no imaginary frequencies, indicating the dynamical stability of VSiGeN<sub>4</sub>. *Ab initio* molecular dynamics simulations are further performed to examine the thermal stability of VSiGeN<sub>4</sub> on a  $4 \times 4 \times 1$  supercell with a Nose thermostat set to 300 K and a step time of 1 fs. As shown in Fig. 1(d), during the 8 ps simulation time, the energy fluctuates around the equilibrium values without any sudden changes with small distortions in the final configurations, indicating its good thermal stability. VSiGeN<sub>4</sub> has two independent elastic constants,  $C_{11}$  and  $C_{12}$ . If they satisfy Born criteria of  $C_{11} > 0$  and  $C_{11} - C_{12} > 0$  [39,40], VSiGeN<sub>4</sub> will be mechanically stable. The calculated independent elastic constants of VSiGeN<sub>4</sub> are  $C_{11} = 434.15 \text{ N m}^{-1}$  and  $C_{12} = 125.39 \text{ N m}^{-1}$ , which satisfy the Born criteria of mechanical stability, confirming its mechanical stability.

#### IV. ELECTRONIC STRUCTURES

The magnetic anisotropy has crucial effects on the electronic states of 2D materials [4–7]. It is well known that the magnetization is a pseudovector. And then the out-of-plane FM breaks all possible vertical mirrors of the system but preserves the horizontal mirror symmetry. The preserved horizontal mirror symmetry allows spontaneous valley polarization and a nonvanishing Chern number of a 2D system [4]. Although the magnetocrystalline direction of the VSiGeN<sub>4</sub> monolayer is in plane, this can be easily transformed into out of plane by an external magnetic field due to the very small MAE.

For the VSiGeN<sub>4</sub> monolayer, the spin-polarized band structures using both GGA+ $U$  and GGA+ $U$ +SOC are shown in Fig. 2. Figure 2(a) shows a distinct spin splitting due to the exchange interaction, and VSiGeN<sub>4</sub> is a direct narrow band gap semiconductor with a gap value of 0.242 eV. The valence band maximum (VBM) and conduction band minimum (CBM) are at the  $K$  and  $-K$  points, which are provided by the spin up. The energies of the  $-K$  and  $K$  valleys are degenerate for both conduction and valence bands. The V  $d$  orbitals lie in a trigonal prismatic crystal field environment, and the  $d$

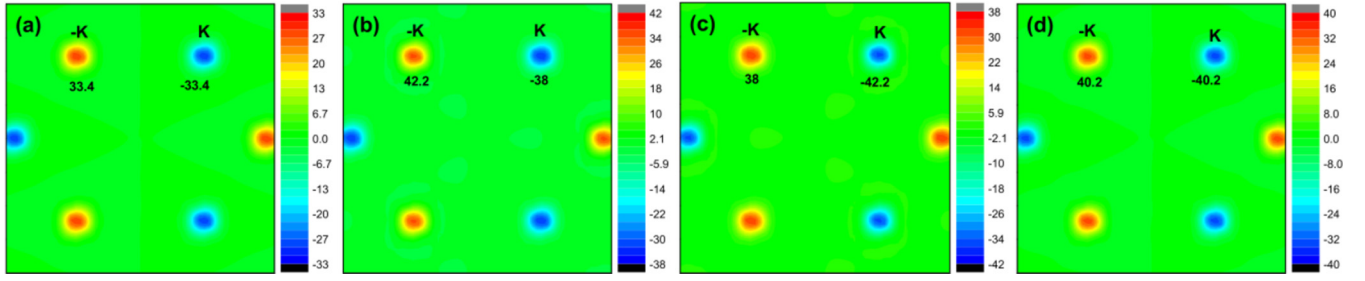


FIG. 3. For the VSIGeN<sub>4</sub> monolayer, the corresponding Berry curvature distribution in the 2D BZ (a) without SOC and (b)–(d) with SOC for the magnetic moment of V along the positive  $z$ , negative  $z$ , and positive  $x$  directions, respectively.

orbitals split into a low-lying  $d_z^2$  orbital and  $d_{xy} + d_{x^2-y^2}$  and  $d_{xz} + d_{yz}$  orbitals. According to the projected band structure in Fig. 3 [30], only the top  $d_z^2$ -dominated valence band in the spin-up direction is occupied by one electron. This is expected to lead to a magnetic moment of  $1\mu_B$  for each V atom, which conforms to the calculated value of  $1.1\mu_B$ .

When including SOC, the valley polarization can be induced with out-of-plane magnetic anisotropy, as shown in Fig. 2(b). The valley splitting of the bottom conduction band is 67 meV, while the valley splitting of the top valence band is only 2 meV. For the bottom conduction band, the energy of the  $K$  valley is higher than that of the  $-K$  valley. As plotted in Fig. 2(c), the valley polarization can be switched by reversing the magnetization direction. (The energy of the  $-K$  valley is higher than that of the  $K$  valley.) Figures 2(b) and 2(c) show that the gap value of VSIGeN<sub>4</sub> is about 0.10 eV. Based on Fig. 2(d), no valley polarization can be observed with in-plane magnetic anisotropy, and it is still a direct band gap semiconductor (0.134 eV).

Figure 3 [30] shows that the  $d_{x^2-y^2} + d_{xy}$  ( $d_z^2$ ) orbitals dominate the  $-K$  and  $K$  valleys of the bottom conduction band (top valence band), which determines the strength of the valley splitting. The intra-atomic interaction  $\hat{H}_{\text{SOC}}^0$  from SOC mainly gives rise to valley polarization, which with out-of-plane magnetization can be expressed as [41–43]

$$\hat{H}_{\text{SOC}}^0 = \alpha \hat{L}_z, \quad (5)$$

where  $\hat{L}_z$  and  $\alpha$  are the orbital angular moment along the  $z$  direction and coupling strength. The resulting energy of the  $K$  or  $-K$  valley can be written as

$$E^\tau = \langle \phi^\tau | \hat{H}_{\text{SOC}}^0 | \phi^\tau \rangle, \quad (6)$$

where  $|\phi^\tau\rangle$  (superscript  $\tau = \pm 1$  is the valley index) indicates the orbital basis for the  $-K$  or  $K$  valley. If  $d_{x^2-y^2} + d_{xy}$  orbitals dominate the  $-K$  and  $K$  valleys, the valley splitting  $|\Delta E|$  can be written as

$$|\Delta E| = E^K - E^{-K} = 4\alpha. \quad (7)$$

If the  $-K$  and  $K$  valleys are mainly from  $d_z^2$  orbitals, the valley splitting  $|\Delta E|$  is written as

$$|\Delta E| = E^K - E^{-K} = 0. \quad (8)$$

According to Fig. 3 [30], the valley splitting of the bottom conduction band will be very large, and the valley splitting of the top valence band will be very small, which agrees well with our calculated results. With general magnetization orientation,  $\Delta E = 4\alpha \cos\theta$  [43] ( $\theta = 0^\circ$  and  $90^\circ$  denote

out-of-plane and in-plane directions) for the  $(d_{x^2-y^2} + d_{xy})$ -dominated  $-K/K$  valley. For the in-plane one, the valley splitting of VSIGeN<sub>4</sub> will be zero.

When an in-plane longitudinal electric field  $E$  is applied, Bloch electrons can attain an anomalous velocity  $v$ , which is associated with Berry curvature  $\Omega(k)$ :  $v \sim E \times \Omega(k)$  [44]. The calculated Berry curvatures of VSIGeN<sub>4</sub> as a contour map in the 2D BZ with and without SOC are plotted in Fig. 3, and their hot spots are around the  $-K$  and  $K$  valleys. The four situations all show that Berry curvatures have opposite signs around the  $-K$  and  $K$  valleys with equal (unequal) magnitudes for the valley-nonpolarized (valley-polarized) situation. When reversing the magnetization from the  $z$  to  $-z$  direction, the signs of Berry curvature at the  $-K$  and  $K$  valleys remain unchanged, but their magnitudes are exchanged with one another. When the Fermi level falls between the  $-K$  and  $K$  valleys with appropriate electron doping, the Berry curvature forces the spin-up carriers of the  $K$  valley to accumulate on one side of the sample by an applied in-plane electric field, giving rise to an anomalous valley Hall effect. When the magnetization is reversed, the spin-down carriers of the  $-K$  valley move to another side of the sample due to the opposite Berry curvature compared with that of the  $K$  valley.

## V. STRAIN EFFECTS

Strain is an effective method to tune the electronic state of some 2D materials and can produce novel electronic states, such as FV, QAH, and HVM states [7,9,10]. We use  $a/a_0$  to simulate the biaxial strain, where  $a$  and  $a_0$  are the strained and unstrained lattice constants, respectively. Here, both compressive ( $a/a_0 < 1$ ) and tensile ( $a/a_0 > 1$ ) strains are applied to achieve electronic state tuning ( $a/a_0 = 0.96$ – $1.04$ ). As shown in Fig. 4, the total energy differences between AFM and FM ordering using a rectangle supercell indicate that the FM state is always the magnetic ground state of VSIGeN<sub>4</sub> in the considered strain range. It is found that total energy differences between AFM and FM ordering at  $a/a_0 = 1.03$  have a sudden jump. To explain this, the energies of AFM and FM ordering as a function of  $a/a_0$  are plotted in Fig. 4 [30]. The calculated results show that the energy of AFM ordering suddenly increases at  $a/a_0 = 1.03$ . To further reveal the underlying causes, the magnetic moments of the V atom for both AFM and FM ordering as a function of  $a/a_0$  are plotted in Fig. 5 [30]. The energy difference jump is due to an abrupt change in the magnetic moment of the V atom for AFM ordering, which reduces the magnetic interaction energy.

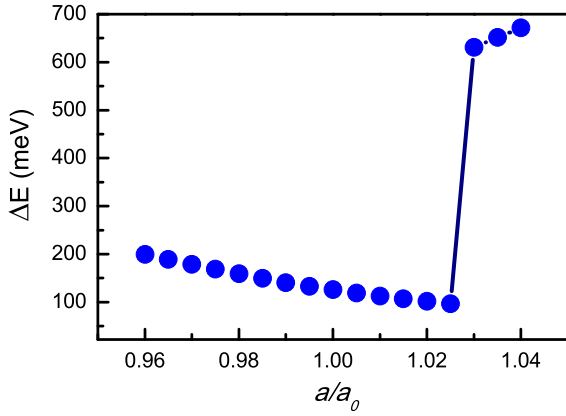


FIG. 4. For the VSiGeN<sub>4</sub> monolayer, the energy differences  $\Delta E$  between AFM and FM ordering as a function of  $a/a_0$ .

Next, the strain effects on the electronic structures of VSiGeN<sub>4</sub> are investigated. First, the total energy band gaps as a function of  $a/a_0$  without SOC are plotted in Fig. 5, and energy band structures at some representative  $a/a_0$  values are shown in Fig. 6 [30]. When  $a/a_0$  changes from 0.96 to 1.04, the gap first closes at about  $a/a_0 = 0.987$  and then continues to increase. Before the energy gap closes, VSiGeN<sub>4</sub> is a direct gap semiconductor with both VBM and CBM at the  $K$  or  $-K$  point. When  $a/a_0 > 0.987$ , VSiGeN<sub>4</sub> is still a direct gap semiconductor at small  $a/a_0$ . When  $a/a_0 > 1.01$ , VSiGeN<sub>4</sub> is an indirect gap semiconductor. The CBM is at the  $K/-K$  point, whereas the VBM deviates slightly from the  $\Gamma$  point. In the considered strain range, the  $K$  and  $-K$  valleys are always provided by the spin up.

When including SOC, the magnetic anisotropy has crucial effects on the electronic structures of VSiGeN<sub>4</sub>. First, we consider that the magnetocrystalline direction of VSiGeN<sub>4</sub> is out of plane. At some representative  $a/a_0$  values, the energy band structures with GGA+ $U$ +SOC are plotted in Fig. 7 [30], and the evolutions of the total energy band gap along with those at the  $-K/K$  point vs  $a/a_0$  are shown in Fig. 5. Calculated results show that there are two points around  $a/a_0 = 0.9925$  and  $0.9945$ , where the total energy band gap is closed. At the two strain points, conduction electrons are intrinsically 100% valley polarized, and the HVM state can be realized [45]. At about  $a/a_0 = 0.9925$ , the band gap of the  $K$  valley gets closed, while a band gap at the  $-K$  valley can be observed. At about  $a/a_0 = 0.9945$ , the band gap at the  $-K$  valley is zero, while the band gap of the  $K$  valley is kept. The considered strain ( $a/a_0$ ) region can be divided into three parts by two HVM electronic states.

It is found that the  $K$  and  $-K$  valleys of both the valence and conduction bands are primarily contributed by the  $d_{x^2-y^2} + d_{xy}$  or  $d_{z^2}$  orbitals of V atoms, and the orbital characters' energy band structures at representative values of  $a/a_0 = 0.97$ ,  $0.993$ , and  $1.02$  from three regions are plotted in Fig. 6. For  $0.96 < a/a_0 < 0.9925$ , the  $d_{x^2-y^2} + d_{xy}$  orbitals dominate the  $K$  and  $-K$  valleys of the valence bands, while the two valleys of the conduction bands are mainly from  $d_{z^2}$  orbitals (for example,  $a/a_0 = 0.97$ ). When  $a/a_0$  is between  $0.9925$  and  $0.9945$ , the  $d_{x^2-y^2} + d_{xy}/d_{z^2}$  orbitals dominate the  $K$  valleys of conduction and valence bands, while the orbital characters of the  $-K$  valley remain unchanged (for example,

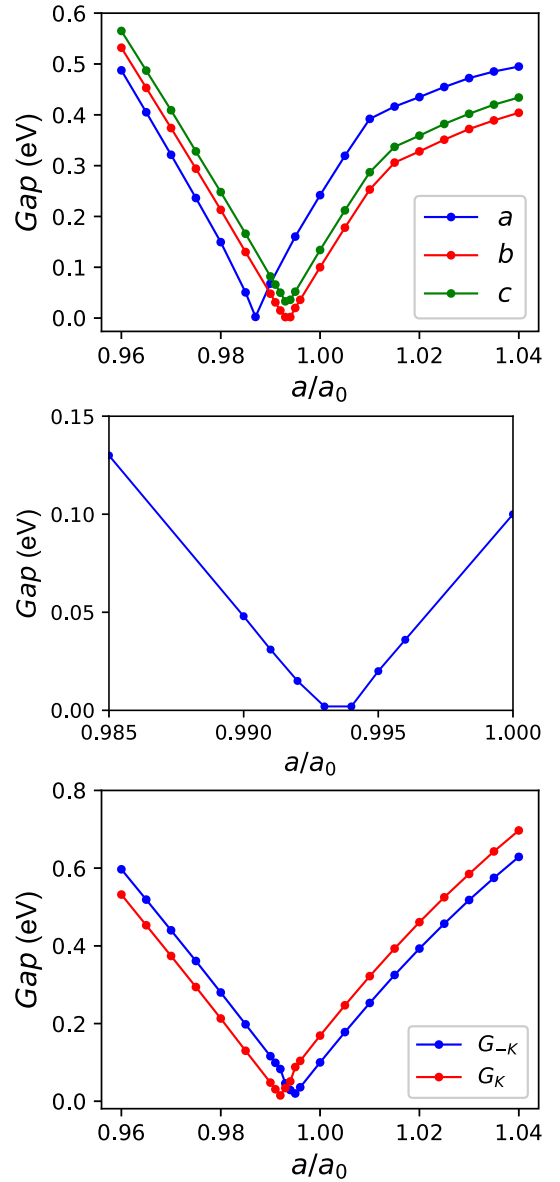


FIG. 5. Top: the global energy band gap without SOC (line a) and with SOC (out-of-plane magnetic anisotropy (line b) and in-plane magnetic anisotropy (line c)). Middle: an enlarged view of the global energy band gap with SOC (out-of-plane magnetic anisotropy) near  $a/a_0 = 0.993$ . Bottom: the energy band gaps for the  $-K$  and  $K$  valleys as a function of  $a/a_0$  with SOC (out-of-plane magnetic anisotropy).

$a/a_0 = 0.993$ ). For  $0.9945 < a/a_0 < 1.04$ , the distributions of  $d_{x^2-y^2} + d_{xy}$  and  $d_{z^2}$  orbitals are opposite to those of  $0.96 < a/a_0 < 0.9925$  (for example,  $a/a_0 = 1.02$ ). This means that there is two-time band inversion between the  $d_{xy} + d_{x^2-y^2}$  and  $d_{z^2}$  orbitals with increasing  $a/a_0$ . The first occurs in the  $K$  valley, accompanied by the first HVM state. The second band inversion occurs in the  $-K$  valley, along with the second HVM state.

The two HVM states imply that the total gap of VSiGeN<sub>4</sub> closes and reopens two times, which suggests a topological phase transition along with band inversion between the  $d_{xy} + d_{x^2-y^2}$  and  $d_{z^2}$  orbitals. The QAH state may appear

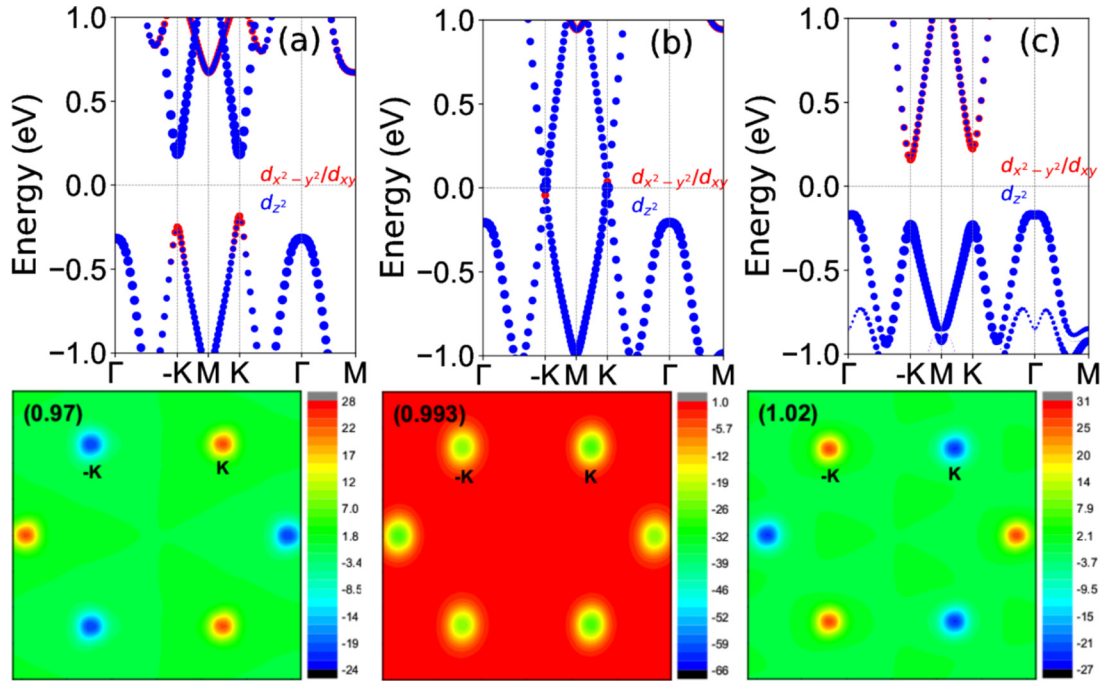


FIG. 6. For the VSiGeN<sub>4</sub> monolayer with out-of-plane magnetic anisotropy, the V  $d_{x^2-y^2} + d_{xy}$  and  $d_{z^2}$  orbital character energy band structures at representative (a)  $a/a_0 = 0.97$ , (b) 0.993, and (c) 1.02, along with the corresponding Berry curvature distribution in the 2D BZ.

when  $a/a_0$  is between 0.9925 and 0.9945. The edge states at a representative value of  $a/a_0 = 0.993$  are calculated to confirm the QAH phase, which is plotted in Fig. 7. It is clearly seen that a nontrivial chiral edge state connects the conduction bands and valence bands, implying a QAH phase. The calculated Chern number  $C = -1$ , which is also obtained by integrating the Berry curvature (see Fig. 6) within the first BZ. There are no nontrivial chiral edge states for the other two regions ( $0.96 < a/a_0 < 0.9925$  and  $0.9945 < a/a_0 < 1.04$ ). With increasing  $a/a_0$ , two-time topological phase transitions can be observed in monolayer VSiGeN<sub>4</sub>.

The transformations of Berry curvatures of the  $K$  and  $-K$  valleys are related to these topological phase transitions, and the distributions of Berry curvature are plotted in Fig. 6 at representative values of  $a/a_0 = 0.97$ , 0.993, and 1.02. For

$0.96 < a/a_0 < 0.9925$  and  $0.9945 < a/a_0 < 1.04$ , the Berry curvatures around the  $-K$  and  $K$  valleys have opposite signs and different magnitudes. However, for  $0.9925 < a/a_0 < 0.9945$ , the same signs and different magnitudes can be observed for Berry curvatures around the  $-K$  and  $K$  valleys. When  $a/a_0$  changes from 0.96 to 1.04, there are two topological phase transitions, which are related to the flipping of the sign of the Berry curvature at the  $-K$  or  $K$  valley. For the first topological phase transitions, the positive Berry curvature ( $a/a_0 = 0.97$ ) changes into a negative one ( $a/a_0 = 0.993$ ) at the  $K$  valley. The second topological phase transition is related to the sign flipping of the Berry curvature of the  $-K$  valley, and the negative Berry curvature ( $a/a_0 = 0.993$ ) changes into a positive one ( $a/a_0 = 1.02$ ). These results suggest that strain can induce sign-reversible Berry curvature at the  $K$  or  $-K$  valley, and this is relevant to the topological phase transition.

The calculated results show that the VSiGeN<sub>4</sub> monolayer has spontaneous valley polarization, and the valley splitting for both valence and conduction bands is plotted in Fig. 8. For  $0.96 < a/a_0 < 0.9925$ , the valley splitting of the valence band is noteworthy, while the valley splitting of the conduction band is very small. However, for  $0.9945 < a/a_0 < 1.04$ , the opposite situation can be observed for valley splitting compared with the case of  $0.96 < a/a_0 < 0.9925$ . These results can be explained by the distributions of  $d_{x^2-y^2} + d_{xy}$  and  $d_{z^2}$  orbitals (see Fig. 6). If  $d_{x^2-y^2} + d_{xy}$  ( $d_{z^2}$ ) orbitals dominate the  $-K$  and  $K$  valleys, the valley splitting will be large (small). For  $0.9925 < a/a_0 < 0.9945$ , the valley splitting for both valence and conduction bands is observable. In this region, VSiGeN<sub>4</sub> is a VQAH with spontaneous valley splitting and chiral edge states. For VQAH, the edge state has a special behavior of chiral-spin-valley locking. For example, for  $a/a_0 = 0.993$ , the edge state in Fig. 7 is spin up with 100% spin polarization and 100% valley polarization, which

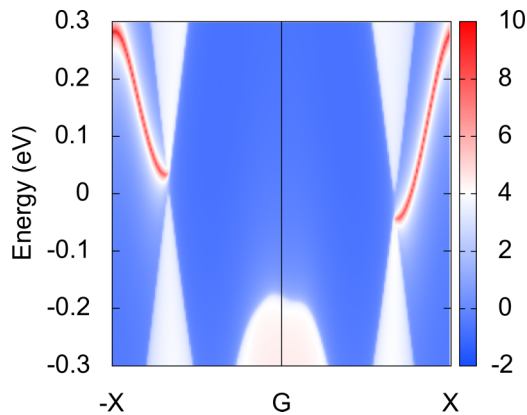


FIG. 7. For the VSiGeN<sub>4</sub> monolayer with out-of-plane magnetic anisotropy, the topological edge states at representative  $a/a_0 = 0.993$ .

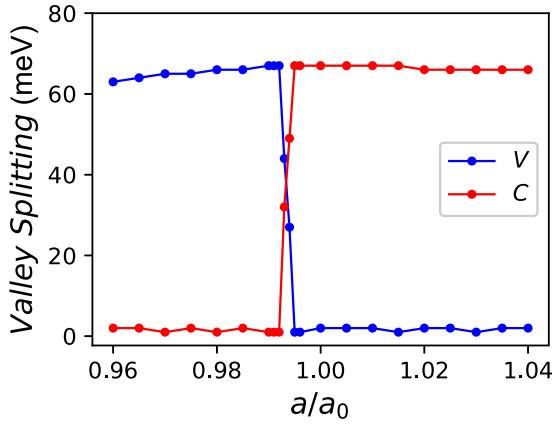


FIG. 8. For the VSiGeN<sub>4</sub> monolayer with out-of-plane magnetic anisotropy, the absolute value of valley splitting in both conduction (C) and valence (V) bands as a function of  $a/a_0$ .

is because the bands near the Fermi level are dominated by spin-up bands. The edge state only appears at the  $K$  valley due to the flipping of the sign of the Berry curvature or band inversion at the  $K$  valley. When the magnetization is reversed, the edge state will move to the  $-K$  valley with an opposite spin direction and chirality.

In quick succession, we suppose the magnetocrystalline direction of the VSiGeN<sub>4</sub> monolayer is along the in-plane one. The energy band gaps as a function of  $a/a_0$  are plotted in Fig. 5, and the representative energy band structures are shown in Fig. 8 [30]. When  $a/a_0$  changes from 0.96 to 1.04, the gap first decreases and then increases. The corresponding  $a/a_0$  of gap closing is about 0.993. It is found that no spontaneous valley polarization in both the valence and conduction bands can be observed, and no QAH phase can be induced by strain. When  $a/a_0$  is less than about 1.01, except for a value of 0.993 (semimetal), VSiGeN<sub>4</sub> is a direct gap semiconductor with both VBM and CBM at the  $K$  or  $-K$  point. When  $a/a_0 > 1.01$ , VSiGeN<sub>4</sub> is an indirect gap semiconductor with the CBM at the  $K/-K$  points, and the VBM deviates slightly from the  $\Gamma$  point. In short, the VSiGeN<sub>4</sub> monolayer is a common FM semiconductor or semimetal.

Finally, we investigate the strain effects on MAE of VSiGeN<sub>4</sub>. We plot the MCA energy as a function of  $a/a_0$  in Fig. 9. Strain-driven complex MCA (multiple transitions in the MCA) can be observed. In the considered strain range, the MSA energy changes from  $-19$  to  $-17$  to  $-15$   $\mu\text{eV}$  when  $a/a_0$  changes from 0.96 to 1.00 to 1.04. The calculated results show that the MAE is always negative within the considered strain range, which means that strained VSiGeN<sub>4</sub> is an intrinsically common magnetic semiconductor. However, the magnetization can be adjusted from the in-plane to the off-plane direction by overcoming a small energy barrier by using the external magnetic field, which will produce valley polarization and a QAH phase. Within the considered strain range, the largest energy barrier (56  $\mu\text{eV}$  at  $a/a_0 = 0.96$ ) is equivalent to applying an external magnetic field of around 0.28–0.56 T.

## VI. DISCUSSION AND CONCLUSION

Monolayer RuBr<sub>2</sub> shows the same electronic states induced by strain as VSiGeN<sub>4</sub> for both out-of-plane and in-plane cases

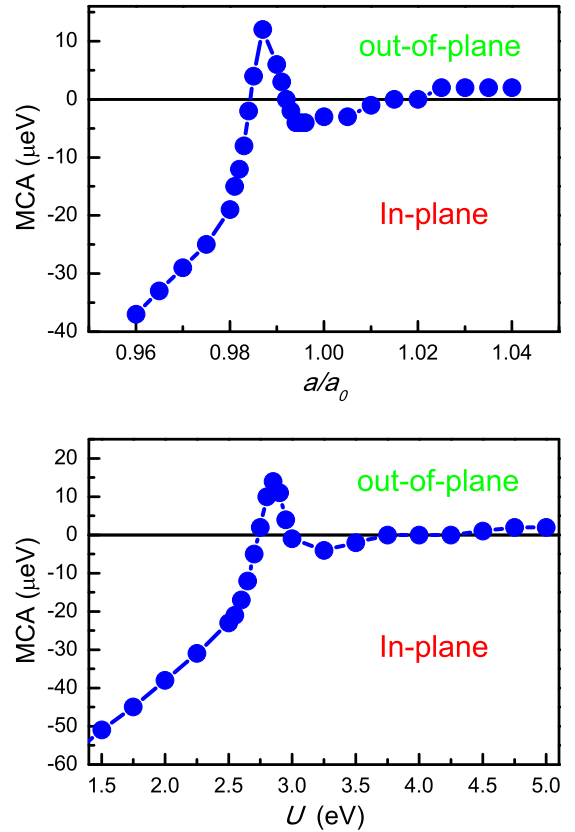


FIG. 9. For the VSiGeN<sub>4</sub> monolayer, the MCA energy as a function of  $a/a_0$  (top panel) and  $U$  (bottom panel).

[7]. However, the MCA energy of RuBr<sub>2</sub> varies monotonously with increasing  $a/a_0$ . The strain can suppress (enhance) the kinetic energy of the electron and then effectively enhance (suppress) the correlation effect [5]. This means that electronic correlation can induce a similar change of the electronic states and MCA energy with strain, which has been confirmed for RuBr<sub>2</sub> [7]. To further confirm the complex strain dependence of the MCA energy, we calculate the MCA energy as a function of correlation strength  $U$ , which is also plotted in Fig. 9. It is clearly seen that MCA vs  $a/a_0$  and MCA vs  $U$  show very similar behaviors, as expected. The complex strain dependence of MCA can be readily extended to VSi<sub>2</sub>P<sub>4</sub>, VSi<sub>2</sub>N<sub>4</sub>, VSiSnN<sub>4</sub>, and so on because they have the same crystal structure as VSiGeN<sub>4</sub>. In fact, for VSi<sub>2</sub>P<sub>4</sub>, one can observe similar transitions in the MCA energy as a function of  $U$  [5].

In summary, we have demonstrated that strain can result in a different phase diagram for different magnetic anisotropies (out-of-plane and in-plane cases). For the out-of-plane situation, the strain can induce novel VQAH with exotic chiral-spin-valley locking edge states between two HVM states, and they are related to sign-reversible Berry curvature and band inversions of the  $d_{xy} + d_{x^2-y^2}$  and  $d_{z^2}$  orbitals at the  $-K$  and  $K$  valleys. For the in-plane situation, VSiGeN<sub>4</sub> is a common magnetic semiconductor without spontaneous valley polarization. Particularly, the calculated intrinsic MCA energy shows multiple transitions induced by strain, which is further confirmed by calculating MCA vs  $U$ . Intrinsically, there is not a VQAH, which can be realized by the external magnetic

field. Our work deepens our understanding of strain effects in the V-based 2D  $MA_2Z_4$  family of materials and opens different perspectives on multifunctional electronic device applications based on these materials.

#### ACKNOWLEDGMENTS

This work is supported by the Natural Science Basis Research Plan in Shaanxi Province of China (Grant No.

2021JM-456), Graduate Innovation Fund Project in Xi'an University of Posts and Telecommunications (Grant No. CXJJDL2021001), and the National Natural Science Foundation of China (Grant No. 12104130). Y.-S.A. is supported by the Singapore Ministry of Education Academic Research Fund Tier 2 (Grant No. MOE-T2EP50221-0019). We are grateful to the Shanxi Supercomputing Center of China, and the calculations were performed on TianHe-2.

- 
- [1] N. D. Mermin and H. Wagner, *Phys. Rev. Lett.* **17**, 1133 (1966).
- [2] C. Gong, L. Li, Z. Li, H. Ji, A. Stern, Y. Xia, T. Cao, W. Bao, C. Wang, Y. Wang, Z. Q. Qiu, R. J. Cava, S. G. Louie, J. Xia, and X. Zhang, *Nature (London)* **546**, 265 (2017).
- [3] B. Huang, G. Clark, E. Navarro-Moratalla, D. R. Klein, R. Cheng, K. L. Seyler, D. Zhong, E. Schmidgall, M. A. McGuire, D. H. Cobden, W. Yao, D. Xiao, P. Jarillo-Herrero, and X. Xu, *Nature (London)* **546**, 270 (2017).
- [4] X. Liu, H. C. Hsu, and C. X. Liu, *Phys. Rev. Lett.* **111**, 086802 (2013).
- [5] S. Li, Q. Q. Wang, C. M. Zhang, P. Guo, and S. A. Yang, *Phys. Rev. B* **104**, 085149 (2021).
- [6] S. D. Guo, J. X. Zhu, M. Y. Yin, and B. G. Liu, *Phys. Rev. B* **105**, 104416 (2022).
- [7] S. D. Guo, W. Q. Mu, and B. G. Liu, *2D Mater.* **9**, 035011 (2022).
- [8] S. Yang, Y. Chen, and C. Jiang, *InfoMat.* **3**, 397 (2021).
- [9] Y. L. Wang and Y. Ding, *Appl. Phys. Lett.* **119**, 193101 (2021).
- [10] H. Huan, Y. Xue, B. Zhao, G. Y. Gao, H. R. Bao, and Z. Q. Yang, *Phys. Rev. B* **104**, 165427 (2021).
- [11] Y. L. Hong, Z. B. Liu, L. Wang, T. Y. Zhou, W. Ma, C. Xu, S. Feng, L. Chen, M. L. Chen, D. M. Sun, X. Q. Chen, H. M. Cheng, and W. C. Ren, *Science* **369**, 670 (2020).
- [12] L. Wang, Y. Shi, M. Liu, A. Zhang, Y.-L. Hong, R. Li, Q. Gao, M. Chen, W. Ren, H.-M. Cheng, Y. Li, and X.-Q. Chen, *Nat. Commun.* **12**, 2361 (2021).
- [13] Q. Wang, L. M. Cao, S. J. Liang, W. K. Wu, G. Z. Wang, C. H. Lee, W. L. Ong, H. Y. Yang, L. K. Ang, S. A. Yang, and Y. S. Ang, *npj 2D Mater. Appl.* **5**, 71 (2021).
- [14] L. Cao, G. Zhou, Q. Wang, L. K. Ang, and Y. S. Ang, *Appl. Phys. Lett.* **118**, 013106 (2021).
- [15] S. D. Guo, W. Q. Mu, Y. T. Zhu, R. Y. Han, and W. C. Ren, *J. Mater. Chem. C* **9**, 2464 (2021).
- [16] S. D. Guo, Y. T. Zhu, W. Q. Mu, and X. Q. Chen, *J. Mater. Chem. C* **9**, 7465 (2021).
- [17] D. Dey, A. Ray, and L. P. Yu, *Phys. Rev. Materials* **6**, L061002 (2022).
- [18] P. Hohenberg and W. Kohn, *Phys. Rev.* **136**, B864 (1964); W. Kohn and L. J. Sham, *ibid.* **140**, A1133 (1965).
- [19] G. Kresse, *J. Non-Cryst. Solids* **192–193**, 222 (1995).
- [20] G. Kresse and J. Furthmüller, *Comput. Mater. Sci.* **6**, 15 (1996).
- [21] G. Kresse and D. Joubert, *Phys. Rev. B* **59**, 1758 (1999).
- [22] J. P. Perdew, K. Burke, and M. Ernzerhof, *Phys. Rev. Lett.* **77**, 3865 (1996).
- [23] S. L. Dudarev, G. A. Botton, S. Y. Savrasov, C. J. Humphreys, and A. P. Sutton, *Phys. Rev. B* **57**, 1505 (1998).
- [24] A. Togo, F. Oba, and I. Tanaka, *Phys. Rev. B* **78**, 134106 (2008).
- [25] T. Fukui, Y. Hatsugai, and H. Suzuki, *J. Phys. Soc. Jpn.* **74**, 1674 (2005).
- [26] H. J. Kim, <https://github.com/Infant83/VASPBERRY>.
- [27] H. J. Kim, C. Li, J. Feng, J.-H. Cho, and Z. Zhang, *Phys. Rev. B* **93**, 041404(R) (2016).
- [28] A. A. Mostofia, J. R. Yatesb, G. Pizzif, Y.-S. Lee, I. Souzad, D. Vanderbilt, and N. Marzarif, *Comput. Phys. Commun.* **185**, 2309 (2014).
- [29] Q. Wu, S. Zhang, H. F. Song, M. Troyer, and A. A. Soluyanov, *Comput. Phys. Commun.* **224**, 405 (2018).
- [30] See Supplemental Material at <http://link.aps.org/supplemental/10.1103/PhysRevB.106.064416> for energy band fitting, the first BZ with high-symmetry points, V  $d$  orbital characters of the energy bands, the energies and magnetic moment of the V atom for FM and AFM ordering as a function of  $a/a_0$ , and energy band structures at six different  $a/a_0$  values.
- [31] X. B. Lu, R. X. Fei, L. H. Zhu, and L. Yang, *Nat. Commun.* **11**, 4724 (2020).
- [32] M. Akram, H. LaBollita, D. Dey, J. Kapteghian, O. Erten, and A. S. Botana, *Nano Lett.* **21**, 6633 (2021).
- [33] H. J. F. Jansen, *Phys. Rev. B* **59**, 4699 (1999).
- [34] F. Xue, Y. Hou, Z. Wang, and R. Wu, *Phys. Rev. B* **100**, 224429 (2019).
- [35] K. Sheng, Q. Chen, H. K. Yuan, and Z. Y. Wang, *Phys. Rev. B* **105**, 075304 (2022).
- [36] J. L. Lado and J. Fernández-Rossier, *2D Mater.* **4**, 035002 (2017).
- [37] P. Jiang, L. Kang, Y.-L. Li, X. Zheng, Z. Zeng, and S. Sanvito, *Phys. Rev. B* **104**, 035430 (2021).
- [38] S. Zhang, R. Xu, W. Duan, and X. Zou, *Adv. Funct. Mater.* **29**, 1808380 (2019).
- [39] E. Cadelano and L. Colombo, *Phys. Rev. B* **85**, 245434 (2012).
- [40] Y. X. Wu, W. Sun, S. Y. Liu, B. Wang, C. Liu, H. B. Yin, and Z. X. Cheng, *Nanoscale* **13**, 16564 (2021).
- [41] W. Y. Tong, S. J. Gong, X. Wan, and C. G. Duan, *Nat. Commun.* **7**, 13612 (2016).
- [42] P. Zhao, Y. Dai, H. Wang, B. B. Huang, and Y. D. Ma, *ChemPhysMater* **1**, 56 (2022).
- [43] R. Li, J. W. Jiang, W. B. Mi, and H. L. Bai, *Nanoscale* **13**, 14807 (2021).
- [44] D. Xiao, M. C. Chang, and Q. Niu, *Rev. Mod. Phys.* **82**, 1959 (2010).
- [45] H. Hu, W. Y. Tong, Y. H. Shen, X. Wan, and C. G. Duan, *npj Comput. Mater.* **6**, 129 (2020).